Measurement of the Dipole Polarizability of the Unstable Neutron-Rich Nucleus ^{68}Ni

D. M. Rossi,[1,2,*] P. Adrich,[1] F. Aksouh,[1,†] H. Alvarez-Pol,[3] T. Aumann,[4,1,‡] J. Benlliure,[3] M. Böhmer,[5] K. Boretzky,[1] E. Casarejos,[6] M. Chartier,[7] A. Chatillon,[1] D. Cortina-Gil,[3] U. Datta Pramanik,[8] H. Emling,[1] O. Ershova,[9] B. Fernandez-Dominguez,[3,7] H. Geissel,[1] M. Gorska,[1] M. Heil,[1] H. T. Johansson,[10,1] A. Junghans,[11] A. Kelic-Heil,[1] O. Kiselev,[1,2] A. Klimkiewicz,[1,12] J. V. Kratz,[2] R. Krücken,[5] N. Kurz,[1] M. Labiche,[13,14] T. Le Bleis,[1,9,15] R. Lemmon,[14] Yu. A. Litvinov,[1] K. Mahata,[1,16] P. Maierbeck,[5] A. Movsesyan,[4] T. Nilsson,[10] C. Nociforo,[1] R. Palit,[17] S. Paschalis,[4,7] R. Plag,[9,1] R. Reifarth,[9,1] D. Savran,[18,19] H. Scheit,[4] H. Simon,[1] K. Sümmerer,[1] A. Wagner,[11] W. Waluś,[12] H. Weick,[1] and M. Winkler[1]

[1]*GSI Helmholtzzentrum für Schwerionenforschung GmbH, D-64291 Darmstadt, Germany*
[2]*Institut für Kernchemie, Johannes Gutenberg-Universität, D-55128 Mainz, Germany*
[3]*University of Santiago de Compostela, E-15705 Santiago de Compostela, Spain*
[4]*Institut für Kernphysik, Technische Universität Darmstadt, D-64289 Darmstadt, Germany*
[5]*Physik-Department E12, Technische Universität München, D-85748 Garching, Germany*
[6]*University of Vigo, E-36310 Vigo, Spain*
[7]*University of Liverpool, Liverpool L69 7ZE, United Kingdom*
[8]*Saha Institute of Nuclear Physics, Kolkata 700-064, India*
[9]*Institut für Angewandte Physik, Goethe Universität, D-60438 Frankfurt am Main, Germany*
[10]*Chalmers University of Technology, SE-41296 Göteborg, Sweden*
[11]*Helmholtz-Zentrum Dresden-Rossendorf e.V., D-01328 Dresden, Germany*
[12]*Jagiellonian University, PL-30-059 Krakow, Poland*
[13]*University of the West of Scotland, Paisley PA1 2BE, United Kingdom*
[14]*STFC Daresbury Laboratory, Warrington WA4 4AD, United Kingdom*
[15]*Institut Pluridisciplinaire Hubert Curien, F-67037 Strasbourg, France*
[16]*Bhabha Atomic Research Centre, Mumbai 400-085, India*
[17]*Tata Institute of Fundamental Research, Mumbai 400-005, India*
[18]*ExtreMe Matter Institute EMMI and Research Division, GSI Helmholtzzentrum für Schwerionenforschung GmbH, D-64291 Darmstadt, Germany*
[19]*Frankfurt Institute for Advanced Studies, D-60438 Frankfurt am Main, Germany*

(Received 12 September 2013; published 10 December 2013)

The $E1$ strength distribution in ^{68}Ni has been investigated using Coulomb excitation in inverse kinematics at the R^{3}B-LAND setup and by measuring the invariant mass in the one- and two-neutron decay channels. The giant dipole resonance and a low-lying peak (pygmy dipole resonance) have been observed at 17.1(2) and 9.55(17) MeV, respectively. The measured dipole polarizability is compared to relativistic random phase approximation calculations yielding a neutron-skin thickness of 0.17(2) fm. A method and analysis applicable to neutron-rich nuclei has been developed, allowing for a precise determination of neutron skins in nuclei as a function of neutron excess.

DOI: 10.1103/PhysRevLett.111.242503 PACS numbers: 24.30.Cz, 24.30.Gd, 25.60.−t, 25.70.De

The knowledge of the nuclear equation of state (EOS) of neutron-rich matter is key for the understanding of many phenomena both in nuclear physics and astrophysics, ranging from the properties and reactions of neutron-rich nuclei to supernova dynamics and properties of neutron stars. Huge theoretical and experimental efforts have been devoted in recent years to constrain the isospin-asymmetric part of the EOS, i.e., the symmetry energy, and its density dependence, see, e.g., Refs. [1–3]. The neutron skin of neutron-rich nuclei is a property that is directly related to the EOS of asymmetric matter close to saturation density. The density dependence of the symmetry energy governs the neutron skin in nuclei as well as the radius of neutron stars [4]. However, a precise experimental determination of the neutron-skin thickness ($\Delta R_{n,p}$) remains challenging [5,6].

The electric dipole ($E1$) response of nuclei and, in particular, its dependence on the neutron-to-proton asymmetry, is governed by the symmetry energy and its density dependence [7–10]. Recently, the low-lying $E1$ strength appearing in neutron-rich nuclei, often denoted as pygmy dipole resonance (PDR) [11], has been utilized to constrain the symmetry energy or the neutron-skin thickness [7,12,13]. It has been pointed out by Reinhard and Nazarewicz [8] that the electric dipole polarizability α_D of the nucleus provides a more robust and less model-dependent observable to extract $\Delta R_{n,p}$. The dipole polarizability, indeed very sensitive to low-lying $E1$ strength due to its inverse energy weighting, is defined as

$$\alpha_D = \frac{\hbar c}{2\pi^2} \int_0^\infty \frac{\sigma(E)}{E^2} dE, \quad (1)$$

where $\sigma(E)$ is the photoabsorption cross section [9].

Tamii *et al.* measured the dipole polarizability of ^{208}Pb, amounting to 20.1(6) fm$^3/e^2$, and extracted its neutron-skin thickness [5,14]. It has been demonstrated recently by Roca-Maza *et al.* [10] that the mild model dependence of such an approach, as discussed in Ref. [14], can be further reduced by correlating the product of α_D and the symmetry energy at saturation density J with $\Delta R_{n,p}$, yielding a value of $\Delta R_{n,p} = 0.165(26)$ fm for ^{208}Pb. (Here, we added the experimental and theoretical errors given in Ref. [10] quadratically.) The importance of independent measurements of α_D and the parity-violating asymmetry for different nuclei has been pointed out in Ref. [10] as well. One would expect much more stringent constraints from complementary measurements and, in particular, from neutron-skin measurements for unstable neutron-rich nuclei, that provide increased sensitivity due to larger skin thicknesses and which can be measured systematically as a function of neutron excess.

The redistribution of $E1$ strength as a function of neutron-to-proton asymmetry is of great interest also from a nuclear-structure point of view. Considering neutron-rich nuclei, the appearance of low-lying $E1$ strength in the vicinity of the neutron separation threshold has triggered considerable experimental [15] and theoretical [16] efforts in recent years. In contrast to their stable counterparts [5,17–20], experimental evidence of low-lying $E1$ strength (PDR) in unstable nuclei is still scarce [11]. Apart from the particular effect of halo structures on the low-energy response of nuclei at the neutron drip line, the $E1$ strength of unstable nuclei has only been studied for a few cases so far [12,21–25]. From the experimental evidence for the PDR in ^{130}Sn and ^{132}Sn [24] at excitation energies around 10 MeV, exhausting respectively 7(3)% and 4(3)% of the $E1$ energy-weighted sum rule strength (S_{EWSR}), a first attempt was undertaken to determine $\Delta R_{n,p}$ in ^{130,132}Sn [12]. More recently, an experiment using (γ^*, γ') virtual photon scattering—where γ^* represents a virtual photon—to investigate the low-lying $E1$ strength in ^{68}Ni has been carried out [25], revealing $S_{\mathrm{EWSR}} = 5.0(1.5)$% under the assumption of a branching ratio for the direct γ decay of ~4% in the PDR energy region.

In this Letter, we present the first experimental measurement of the dipole polarizability in an unstable neutron-rich nucleus, providing a constraint on $\Delta R_{n,p}$ for ^{68}Ni. This method will allow in the future for a systematic measurement of how the polarizability and neutron skin evolve along isotopic chains, which will be of enormous value to further constrain the isospin-asymmetric part of the EOS. The $E1$ strength in ^{68}Ni was investigated by analyzing the (γ^*, n) and (γ^*, $2n$) channels, allowing us not only to extract the resonance parameters of the PDR and of the isovector giant dipole resonance (GDR), but also to measure for the first time the nonstatistical decay of ^{68}Ni. In addition, a γ-decay branching ratio for the PDR decay could be extracted by comparing our result to a previous measurement [25].

The investigation of the decay of radioactive nuclei excited beyond the particle threshold requires a high-efficiency, high-acceptance and kinematically complete measurement in inverse kinematics. Therefore, the present experiment was performed at the R^{3}B-LAND setup located at the GSI Helmholtzzentrum für Schwerionenforschung GmbH in Darmstadt, Germany. A beam of stable ^{86}Kr at approximately 650 MeV/u was used to produce secondary beams through projectile fragmentation on a 4.2 g/cm^2 Be target with subsequent magnetic separation in the FRS fragment separator [26]. ^{68}Ni was delivered to the experimental area with a midtarget kinetic energy of 502.7 MeV/u. The electromagnetic excitation of ^{68}Ni was achieved by using a 519 mg/cm^2 $^{\mathrm{nat}}$Pb target [27] and the excitation energy was reconstructed using the invariant mass of the interacting system. In order to disentangle the electromagnetic, nuclear, and background components of the measured cross sections, auxiliary measurements were carried out with a 187 mg/cm^2 $^{\mathrm{nat}}$C target and with an empty target frame. The nuclear breakup contribution was determined using the measured data on the $^{\mathrm{nat}}$C target scaled to the nuclear radius of ^{208}Pb [28]. The tracking and identification of the charged species was performed using several detectors along the beam path, providing information on their nuclear charge, mass, and momentum.

Projectilelike neutrons were tracked with the neutron detector LAND [29]. This detector allows for time-of-flight and position measurements of neutrons with a time resolution of $\sigma_t \approx 250$ ps and a detection efficiency of 94% for single 500 MeV neutrons. The photon detection was achieved with a CsI γ-ray detector covering $\sim 2\pi$ in the laboratory frame and consisting of 144 crystals arranged in a barrel geometry, with 12 azimuthal and 12 polar segments surrounding the beam pipe.

The complex detector response for neutrons and γ rays leads to considerable distortions in the various cross section distributions. This has been accounted for in a procedure involving the modeling of the decay of the excited nucleus and the detailed understanding of the neutron and γ-ray detector response functions [28] and introducing a new method based on a simultaneous fit of the measured observables in order to extract an unbiased excitation-energy distribution, as described below. The decay is described according to a statistical model, and a nonstatistical decay component is included in addition. The LAND response functions are obtained from neutron data measured in a calibration experiment. For the CsI γ-ray detector, a GEANT4 simulation is used, describing both the response of the γ decay of the excited projectile (fragment) and the atomic background. The CsI detector used here resulted in a better energy resolution but in a smaller calorimetric efficiency than obtained with the 4π NaI

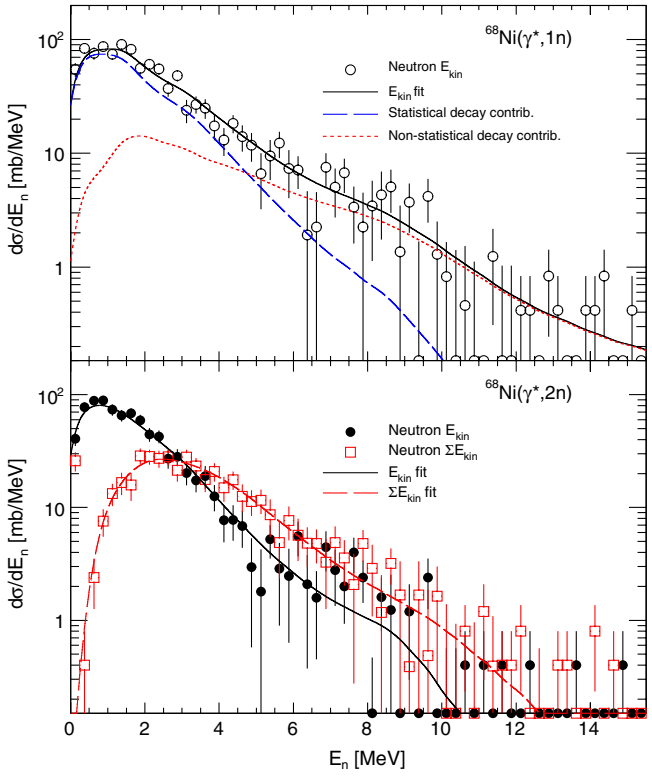

FIG. 1 (color online). Differential cross sections as a function of the neutron kinetic energy for the $(\gamma^*, 1n)$ (upper frame) and $(\gamma^*, 2n)$ (lower frame) channels in the rest frame of the incoming ^{68}Ni. The total neutron kinetic energy (open red squares) for the $(\gamma^*, 2n)$ channel is shown as well in the lower frame. See text for the description of the fit functions.

detector in the Sn experiment [24]. The average of the detected total energy released by photon decay, which is a measure of the calorimetric efficiency of the CsI detector, amounts to approximately 40%.

In Fig. 1, we show the neutron kinetic-energy differential cross sections for the ^{68}Ni(γ^*, n) and ^{68}Ni$(\gamma^*, 2n)$ reaction channels in the rest frame of the projectile. In addition, the sum of the kinetic energies of both neutrons is presented in the lower panel as well, taking the correlation between both evaporated neutrons into account. In order to reconstruct the excitation energy using the invariant mass, the Doppler-corrected γ-ray spectra were also analyzed for these two reaction channels (Fig. 2). The photon spectra of both channels are dominated by the low-energy background originating from atomic interactions between the beam particles and the Pb target. While no strong γ lines in the ^{68}Ni(γ^*, n) channel are observed (inset), the $2^+ \rightarrow 0^+$ (g.s.) transition at 1.42 MeV in ^{66}Ni is clearly visible in the ^{68}Ni$(\gamma^*, 2n)$ data.

In the present analysis, the neutron kinetic energies, the total neutron kinetic energy (in the $2n$ decay channel), and the reconstructed excitation energy were used simultaneously by the fitting algorithm. Establishing an unbiased description of the spectral shape of the $E1$ strength distribution, a series of 8 independent bins (as shown in Fig. 3)

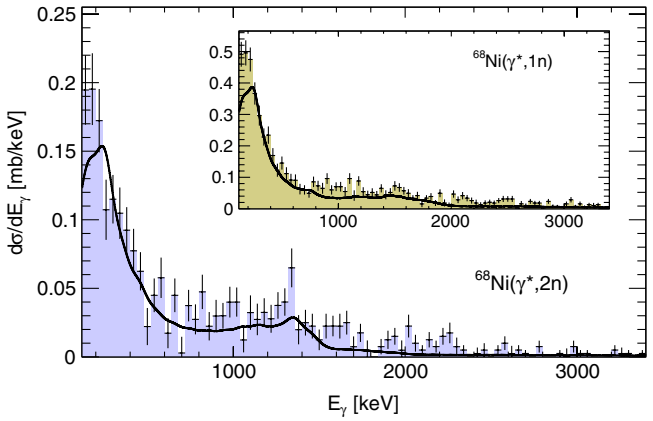

FIG. 2 (color online). Single photon energy spectra for the ^{68}Ni$(\gamma^*, 2n)$ and ^{68}Ni$(\gamma^*, 1n)$ (inset) channels. The respective fit functions are overlaid as black lines.

was used as trial input. The width of each energy bin was derived from the experimental resolution, determined with the previously described simulation. The bins covered the energy regions of the GDR and of eventual low-lying $E1$ strength between the neutron threshold at 7.792 and 28.4 MeV. A χ^2 minimization was performed using the experimental data to adjust the cumulated strength in each bin. The convoluted distributions of the obtained result are shown in Figs. 1 and 2 as the fit functions of the respective observable distributions. With the neutron and photon spectra properly described, the result can be considered as being the deconvoluted excitation-energy distribution and is shown in Fig. 3, with the associated statistical fluctuations and systematic uncertainties arising from correlations among the bins due to the instrumental response discussed above. The resulting spectral shape is robust with respect to variations in the bin width, as long as these values are not chosen to be smaller than the experimental

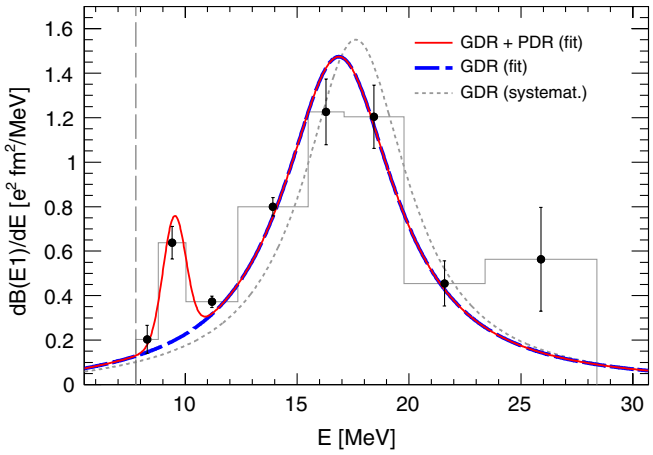

FIG. 3 (color online). $E1$ strength distribution (histogram and black data points) with GDR + PDR fit function (solid red line). The GDR contribution (dashed blue line) and the GDR from systematics (dotted gray line) are shown for reference. The neutron threshold is indicated by the dashed vertical line at 7.792 MeV.

TABLE I. GDR and PDR parameters for ^{68}Ni from fit to $E1$ strength, as shown in Fig. 3. Included as well are the GDR and PDR parameters from the literature.

			This work	Literature	Reference
GDR	E_m	[MeV]	17.1(2)	17.84	[30]
	Γ	[MeV]	6.1(5)	5.69	[30]
	S_{EWSR}	[%]	98(7)	100	
PDR	E_m	[MeV]	9.55(17)	11.0(5)	[25,31]
	σ	[MeV]	0.51(13)	<1	[25]
	S_{EWSR}	[%]	2.8(5)	5.0(1.5)	[13,25]

resolution. Considering the χ^2_ν of the description of the experimental data by the deconvoluted result, we obtain a value of $149.2/162 = 0.92$ for the distribution shown in Fig. 3. Removing the low-lying $E1$ strength increases the value to $\chi^2_\nu = 307.4/162 = 1.90$. Our data also do not reproduce well a PDR at 11 MeV as in Ref. [25], indicated by an increase of χ^2_ν to 1.31.

The neutron kinetic energies in the $1n$ channel cannot be described by a statistical decay alone (dashed line in upper frame in Fig. 1). Since the $2n$ channel opens 5.81 MeV above the $1n$ threshold, neutron energies far above this value are not expected to be observed, unless a second decay mode is considered. By adding a nonstatistical decay component (see Fig. 1) to the fit procedure, in which the excited nucleus decays to the vicinity of the A-1 ground state by the emission of one highly energetic neutron, the neutron kinetic energies in the (γ^*, n) channel can be described properly. The nonstatistical decay branching ratio, considered constant over the energy range including both the GDR and PDR, was obtained from the χ^2 minimization and amounts to 25(2)%, which is in good agreement with the expected values for nuclei in this mass region [30].

In order to extract the GDR and PDR parameters from the $E1$ strength distribution, a function comprising a Breit-Wigner curve and a Gaussian curve was fit to the deconvoluted experimental data. The values obtained for the centroid energy (E_m), width (Γ for the GDR, σ for the PDR), and S_{EWSR} are listed in Table I, which includes the GDR parameters predicted by systematics [30] as well. Figure 3 shows the composite fit function as well as the strength attributed to the GDR alone. A slight shift towards a lower centroid energy is observed for ^{68}Ni compared to the systematics for stable nuclei. Extracting the PDR parameters in this manner allows for a direct comparison with the results obtained by Wieland *et al.* [25], reporting a centroid energy of 11 MeV, a width of less than 1 MeV and $S_{\mathrm{EWSR}} = 5.0(1.5)\%$ (under the assumption of a direct photon decay branching ratio from the PDR region of ~4%). From this comparison, we extract a direct γ-decay branching ratio of 7(2)% for the decay of the PDR in ^{68}Ni, which is significantly larger than the estimate of Ref. [25] assuming a statistical decay. The slight difference of our result compared to the peak energy

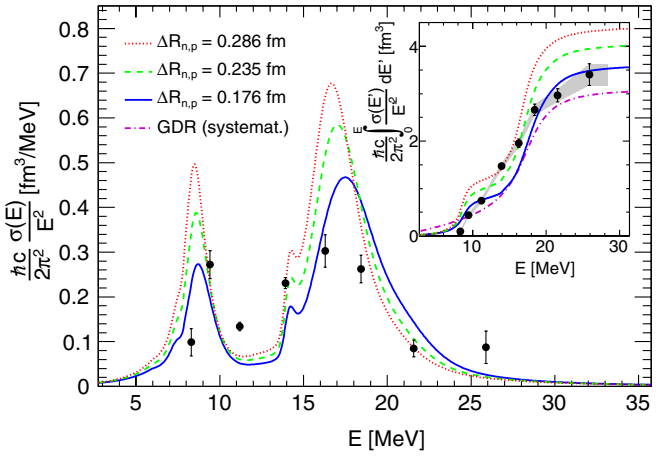

FIG. 4 (color online). Inverse energy-weighted dipole strength (black dots) with FSUGold calculations of Piekarewicz [9] for three neutron-skin thickness values for ^{68}Ni. Inset: Experimental dipole polarizability cumulated sum with corresponding FSUGold calculations. The curve for the GDR from systematics is shown as well for comparison.

of 11.0(5) MeV of Refs. [25,31] might indicate an energy-dependent branching ratio.

We now turn to the extraction of the dipole polarizability α_D, which is enhanced by the PDR in neutron-rich nuclei, as expected for species exhibiting an appreciable neutron skin. Figure 4 presents the experimental inverse energy-weighted dipole strength distribution [integrand of Eq. (1)] of ^{68}Ni compared to the results of a relativistic RPA calculation by Piekarewicz [9], which uses the accurately calibrated FSUGold parametrization of the mean-field interaction. The variation of an empirical coupling constant responsible for isoscalar-isovector mixing leads to a modification of the density dependence of the symmetry energy as well as of the overall $E1$ strength. The tuning of this parameter allows correlations between theoretical and experimental quantities to be established, such as between $\Delta R_{n,p}$ and α_D [9]. The calculated dipole response functions have been convoluted with the experimental energy resolution for comparison. Three cases for different values of $\Delta R_{n,p}$ are shown in Fig. 4 on top of the experimental data.

While the spectral shape of the inverse energy-weighted dipole strength allows us to identify and separate the regions of low-lying and GDR strength, the integral dipole polarizability itself provides sufficient and robust information to correlate $\Delta R_{n,p}$ with an experimental observable. The inset in Fig. 4 depicts the cumulative sum, both for the experimental data as well as for the calculated curves. The experimental value amounts to $\alpha_D = 3.40(23)$ fm^3, evaluated with an upper integration limit of 28.4 MeV. It is interesting to compare the extracted α_D value with the one resulting from the GDR alone (see inset in Fig. 4). The polarizability of ^{68}Ni is about 13% larger than from an assumed GDR strength from systematics, where the largest contribution (~10%) to this difference comes from the PDR.

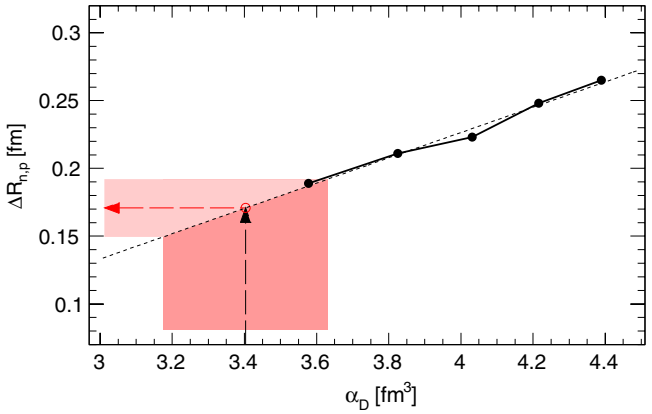

FIG. 5 (color online). Correlation between neutron-skin thickness and dipole polarizability in ^{68}Ni using FSUGold [9]. The shaded zones indicate the experimental errors on the measured α_D and extrapolated $\Delta R_{n,p}$ values.

Making use of the nearly linear relationship between α_D and $\Delta R_{n,p}$ provided by the calculations of Piekarewicz [9] as shown in Fig. 5, we deduce $\Delta R_{n,p} = 0.17(2)$ fm for ^{68}Ni using the measured dipole polarizability. The same calculation which reproduces the measured α_D in ^{68}Ni predicts $\Delta R_{n,p} = 0.15(3)$ fm in ^{208}Pb, which is in very good agreement with the values extracted in Refs. [5,10,14]. Applying the method outlined by Roca-Maza *et al.* [10], excellent agreement is also found with the measured value of α_D for ^{208}Pb [5,10]. A combined analysis, which is beyond the scope of this Letter, will tighten the constraints on the density dependence of the symmetry energy further. In particular, future precise measurements for several neutron-rich nuclei with an appreciable neutron skin using the method presented here will be of great importance.

In summary, we presented results on the $E1$ strength in the neutron-rich ^{68}Ni, with excitation energies spanning the PDR and GDR regions. A bin-wise deconvolution of the experimental data was performed and revealed not only the GDR at its expected location, but also a PDR described by a Gaussian at 9.55(17) MeV exhausting 2.8(5)% of the $E1$ energy-weighted sum rule strength. In combination with a previous measurement [25], a surprisingly large direct photon decay branching ratio for the PDR of 7(2)% has been found. The dipole polarizability was determined from the deconvoluted data for the first time in an unstable nucleus, leading to a value of $\alpha_D = 3.40(23)$ fm^3 integrated up to 28.4 MeV. A comparison of this result with theoretical calculations yielded a neutron-skin thickness of 0.17(2) fm for ^{68}Ni using the measured dipole polarizability. This result can also be compared to the value of 0.200(15) fm deduced by Carbone *et al.* from an analysis of the PDR strength in ^{68}Ni [13]. The method described in this Letter will allow the measurements of the dipole polarizability to be extended to more neutron-rich systems, which will be important to understand and quantify remaining model dependencies and to further constrain the isospin-dependent part of the equation of state of nuclear matter.

We wish to thank J. Piekarewicz for fruitful discussions and for providing numerical data of his calculations from Ref. [9]. This work was supported in part by the Helmholtz International Center for FAIR (HIC for FAIR), the Alliance Program of the Helmholtz Association (HA216/EMMI), the GSI-TU Darmstadt cooperation agreement, the Helmholtz-CAS Joint Research Group HCJRG-108, and BMBF Grants No. 06MZ222I, No. 05P12RDFN8, and No. 06MT9156.

*Present address: National Superconducting Cyclotron Laboratory, Michigan State University, East Lansing, MI 48824, USA.
d.rossi@gsi.de
†Present address: King Saud University, 11451 Riyadh, Saudi Arabia.
‡t.aumann@gsi.de

[1] K. Hebeler, J. M. Lattimer, C. J. Pethick, and A. Schwenk, Astrophys. J. **773**, 11 (2013).
[2] B. A. Li, L.-W. Chen, and C. M. Ko, Phys. Rep. **464**, 113 (2008).
[3] M. B. Tsang *et al.*, Phys. Rev. C **86**, 015803 (2012).
[4] F. J. Fattoyev and J. Piekarewicz, Phys. Rev. C **86**, 015802 (2012).
[5] A. Tamii *et al.*, Phys. Rev. Lett. **107**, 062502 (2011).
[6] S. Abrahamyan *et al.*, Phys. Rev. Lett. **108**, 112502 (2012).
[7] J. Piekarewicz, Phys. Rev. C **73**, 044325 (2006).
[8] P.-G. Reinhard and W. Nazarewicz, Phys. Rev. C **81**, 051303 (2010).
[9] J. Piekarewicz, Phys. Rev. C **83**, 034319 (2011).
[10] X. Roca-Maza, M. Brenna, G. Colò, M. Centelles, X. Viñas, B. K. Agrawal, N. Paar, D. Vretenar, and J. Piekarewicz, Phys. Rev. C **88**, 024316 (2013).
[11] D. Savran, T. Aumann, and A. Zilges, Prog. Part. Nucl. Phys. **70**, 210 (2013).
[12] A. Klimkiewicz *et al.*, Phys. Rev. C **76**, 051603 (2007).
[13] A. Carbone, G. Colò, A. Bracco, L. G. Cao, P. F. Bortignon, F. Camera, and O. Wieland, Phys. Rev. C **81**, 041301 (2010).
[14] J. Piekarewicz, B. K. Agrawal, G. Colò, W. Nazarewicz, N. Paar, P.-G. Reinhard, X. Roca-Maza, and D. Vretenar, Phys. Rev. C **85**, 041302 (2012).
[15] T. Aumann and T. Nakamura, Phys. Scr. **T152**, 014012 (2013).
[16] D. Vretenar, Y. F. Niu, N. Paar, and J. Meng, Phys. Rev. C **85**, 044317 (2012).
[17] D. Savran, M. Fritzsche, J. Hasper, K. Lindenberg, S. Müller, V. Yu. Ponomarev, K. Sonnabend, and A. Zilges, Phys. Rev. Lett. **100**, 232501 (2008).
[18] A. P. Tonchev, S. L. Hammond, J. H. Kelley, E. Kwan, H. Lenske, G. Rusev, W. Tornow, and N. Tsoneva, Phys. Rev. Lett. **104**, 072501 (2010).
[19] J. Endres *et al.*, Phys. Rev. Lett. **105**, 212503 (2010).
[20] R. Schwengner *et al.*, Phys. Rev. C **87**, 024306 (2013).
[21] A. Leistenschneider *et al.*, Phys. Rev. Lett. **86**, 5442 (2001).

[22] E. Tryggestad *et al.*, Phys. Lett. B **541**, 52 (2002).
[23] E. Tryggestad *et al.*, Phys. Rev. C **67**, 064309 (2003).
[24] P. Adrich *et al.*, Phys. Rev. Lett. **95**, 132501 (2005).
[25] O. Wieland *et al.*, Phys. Rev. Lett. **102**, 092502 (2009).
[26] H. Geissel *et al.*, Nucl. Instrum. Methods Phys. Res., Sect. B **70**, 286 (1992).
[27] C. A. Bertulani and G. Baur, Phys. Rep. **163**, 299 (1988).
[28] K. Boretzky *et al.*, Phys. Rev. C **68**, 024317 (2003).
[29] Th. Blaich *et al.*, Nucl. Instrum. Methods Phys. Res., Sect. A **314**, 136 (1992).
[30] M. N. Harakeh and A. van der Woude, *Giant Resonances* (Clarendon Press, Oxford, 2001).
[31] O. Wieland (private communication).